

Models for quasielastic electron and neutrino-nucleus scattering

Carlotta Giusti and Andrea Meucci

Dipartimento di Fisica Nucleare e Teorica, Università degli Studi di Pavia and INFN, Sezione di Pavia, via Bassi 6 I-27100 Pavia, Italy

E-mail: Carlotta.Giusti@pv.infn.it

Abstract. Models developed for the exclusive and inclusive quasielastic (QE) electron-nucleus scattering have been extended to QE neutrino-nucleus scattering. Different descriptions of final-state interactions (FSI) are compared. For the inclusive electron scattering the relativistic Green's function model (RGF) is compared with a model based on the use of relativistic purely real mean field (RMF) potentials in the final state. Both approaches lead to a redistribution of the strength but conserving the total flux. Results for electron and neutrino scattering are presented and discussed in different conditions and kinematics. The results of the RGF and RMF models are compared with the double-differential charged-current QE neutrino cross sections recently measured by the MiniBooNE collaboration using a carbon target.

1. Introduction

Several decades of experimental and theoretical work on electron scattering have provided a wealth of information on nuclear structure and dynamics [1, 2]. Additional information on nuclear properties is in principle available from neutrino-nucleus scattering. The main aim of neutrino experiments, however, is not to investigate nuclear properties, but to determine neutrino properties. In neutrino oscillation experiments neutrino-nucleus scattering is used to detect neutrinos and a proper analysis of data requires that the nuclear response to neutrino interactions is well under control and that the unavoidable theoretical uncertainties on nuclear effects are reduced as much as possible.

Different models developed and successfully tested in comparison with electron-scattering data have been extended to describe nuclear effects in neutrino-nucleus scattering. Although the two situations are different, electron scattering is the best available guide to determine the predictive power of a nuclear model. Nonrelativistic and relativistic models have been developed to describe nuclear effects with different approximations. In general, they can be considered as different and alternative models. Relativity is however important at all energies, in particular at high energies, and in the energy regime of many neutrino experiments a fully relativistic approach is required, where not only relativistic kinematics is considered, but also nuclear dynamics and current operators should be described within a relativistic framework.

Models for the exclusive and inclusive electron and neutrino scattering in the QE region are presented in this contribution. In the QE region the nuclear response is dominated by the mechanism of one-nucleon knockout, where the probe interacts with a quasifree nucleon that is emitted from the nucleus with a direct one-step mechanism and the remaining nucleons

are spectators. In electron-scattering experiments the outgoing nucleon can be detected in coincidence with the scattered electron. In the exclusive $(e, e'p)$ reaction the residual nucleus is left in a specific discrete eigenstate and the final state is completely specified. In the inclusive (e, e') scattering only the scattered electron is detected, the final nuclear state is not determined, and the cross section includes all the available final nuclear states.

For an incident neutrino (antineutrino) neutral-current (NC) and charged-current (CC) scattering can be considered

$$\begin{aligned}\nu(\bar{\nu}) + A &\rightarrow \nu'(\bar{\nu}') + N + (A - 1) && \text{NC} \\ \nu(\bar{\nu}) + A &\rightarrow l^-(l^+) + p(n) + (A - 1) && \text{CC}\end{aligned}$$

In NC scattering only the emitted nucleon can be detected and the cross section is integrated over the energy and angle of the final lepton. Also the state of the residual $(A - 1)$ -nucleus is not determined and the cross section is summed over all the available final states. The same situation occurs for the CC reaction if only the outgoing nucleon is detected. The cross sections are therefore inclusive in the leptonic sector and semi-inclusive in the hadronic sector. The exclusive CC process where the charged final lepton is detected in coincidence with the emitted nucleon can be considered as well. The inclusive CC scattering where only the charged lepton is detected can be treated with the same models used for the inclusive (e, e') reaction.

For all these processes the cross section is obtained in the one-boson exchange approximation from the contraction between the lepton tensor, that under the assumption of the plane-wave approximation for the initial and final lepton wave functions depends only on the lepton kinematics, and the hadron tensor $W^{\mu\nu}$, that contains the nuclear response and whose components are given by bilinear products of the matrix elements of the nuclear current J^μ between the initial and final nuclear states, *i.e.*,

$$W^{\mu\nu} = \sum_f \langle \Psi_f | J^\mu(\mathbf{q}) | \Psi_i \rangle \langle \Psi_i | J^{\nu\dagger}(\mathbf{q}) | \Psi_f \rangle \delta(E_i + \omega - E_f), \quad (1)$$

where ω and \mathbf{q} are the energy and momentum transfer, respectively. Different but consistent models to calculate the components of the hadron tensor in QE electron- and neutrino-nucleus scattering are outlined in the next sections.

2. The exclusive $(e, e'p)$ reaction

For the exclusive $(e, e'p)$ reaction nonrelativistic and relativistic models based on the distorted-wave impulse approximation (DWIA) have been developed to calculate the matrix elements in Eq. (1). The DWIA expression of the matrix elements is the results of the following assumptions [1, 2, 3]:

- i) An exclusive process is considered, where the residual nucleus is left in a discrete eigenstate n of its Hamiltonian.
- ii) The final nuclear state is projected onto the channel subspace spanned by the vectors corresponding to a nucleon, at a given position, and the residual nucleus in the state n . This assumption neglects effects of coupled channels and is justified by the considered asymptotic configuration of the final state.
- iii) The (one-body) nuclear-current operator does not connect different channel subspaces. Thus, also the initial state is projected onto the selected channel subspace. This assumption is the basis of the direct-knockout mechanism and is related to the IA.

The amplitudes of Eq. (1) are then obtained in a one-body representation as

$$\lambda_n^{1/2} \langle \chi^{(-)} | j^\mu(\mathbf{q}) | \varphi_n \rangle, \quad (2)$$

where j^μ the one-body nuclear current, $\chi^{(-)}$ is the single-particle (s.p.) scattering state of the emitted nucleon, φ_n the overlap between the ground state of the target and the final state n , i.e., a s.p. bound state, and the spectroscopic factor λ_n is the norm of the overlap function, that gives the probability of removing from the target a nucleon leaving the residual nucleus in the state n . In the model the s.p. bound and scattering states are consistently derived as eigenfunctions of a non Hermitian energy dependent Feshbach-type optical potential and of its Hermitian conjugate at different energies. In standard DWIA calculations phenomenological ingredients are usually employed: the scattering states are eigenfunctions of a phenomenological optical potential determined through a fit to elastic nucleon-nucleus scattering data and the s.p. bound states are obtained from mean-field potentials, or can be calculated in a phenomenological Woods-Saxon well.

The model can be formulated in a similar way within nonrelativistic DWIA and relativistic RDWIA frameworks [4]. In RDWIA, calculations are performed with a relativistic nuclear-current operator and four-vector relativistic wave functions for the s.p. bound and scattering states. Both DWIA and RDWIA models have been quite successful in describing a large amount of $(e, e'p)$ data in a wide range of nuclei and in different kinematics [2, 4, 5, 6]. The shape of the experimental recoil-momentum distributions corresponding to a particular state of the residual nucleus are well described by model calculations. Then, the spectroscopic factors are usually extracted from the comparison between experimental and theoretical results as the reduction factors that must be applied to the calculated cross sections to reproduce the magnitude of the experimental cross sections.

Recently, the nonrelativistic DWIA and relativistic RDWIA models widely and successfully adopted to describe data in a wide range of stable nuclei have been applied to nuclei with neutron excess, with the aim to study the evolution of the $(e, e'p)$ cross sections as a function of the asymmetry between the number of neutrons and protons [7].

3. Semi-inclusive neutrino-nucleus scattering

For the semi-inclusive NC and CC processes where only the outgoing nucleon is detected, the transition amplitudes can be calculated in the same RDWIA model of Eq. 2. Since the outgoing lepton is not detected, the cross section must be integrated over the energy and angle of the outgoing lepton. The state of the residual nucleus is not determined and the cross section includes all the states n . In the calculations [8, 9, 10] a pure shell-model (SM) description is assumed, i.e., n is a one-hole state and the sum over n is over all the occupied SM states. In [8, 9, 10] FSI are described by a complex optical potential whose imaginary part gives an absorption that reduces the calculated cross section. A similar reduction is found in $(e, e'p)$ calculations. The imaginary part of the optical potential accounts for the fact that in the elastic scattering, if other channels are open besides the elastic one, part of the incident flux is lost in the elastically scattered beam and goes to the inelastic channels that are open. In the exclusive scattering, where only one channel is considered, it is correct to include the absorptive imaginary part of the optical potential and account for the flux lost in the considered channel, but in the inclusive scattering, where all the channels are included, the flux lost in a channel must be found in the other channels, and in the sum over all the channels the flux can be redistributed but must be conserved. Thus, the use of the absorptive imaginary part of the optical potential in the inclusive scattering seems inconsistent with the requirement of flux conservation. For the semi-inclusive process where the emitted nucleon is detected, some of the reaction channels which are responsible for the imaginary part of the potential like multistep processes, fragmentation of the nucleus, etc., are not included in the experimental cross section. There are, however, contributions that are not considered in this model and that can be contained in the experimental cross section. In [8, 9, 10] the semi-inclusive neutrino scattering is treated as a process where the cross section is obtained from the sum of all the integrated exclusive one-nucleon knockout channels. We can expect that

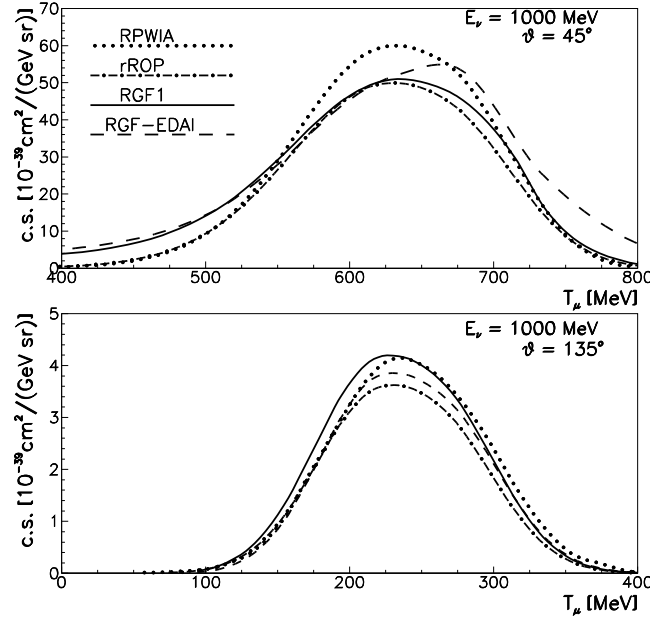


Figure 1. The cross sections of the $^{12}\text{C}(\nu_\mu, \mu^-)$ reaction for an incident neutrino energy of $E_\nu = 1000$ MeV and a muon scattering angle $\vartheta = 45^\circ$ (upper panel) and 135° (lower panel) as a function of the muon kinetic energy T_μ . Results for RPWIA (dotted), rROP (dot-dashed), and the relativistic RGF approach with two different optical potentials [18], i.e., EDAD1 (RGF1) and EDAI (RGF-EDAI), are compared.

the description of FSI by means of a complex optical potential that gives absorption can produce cross sections that are smaller than the experimental data. However, since measurements of cross sections are a hard experimental task, ratios of cross sections have been proposed as alternative quantities that can provide useful informations. In [8, 9, 10] it is shown that ratios of cross sections are less sensitive to distortion effects and several ratios are considered in view of the possible determination of the strange quark content of the nucleon.

4. Inclusive lepton-nucleus scattering

For the inclusive scattering where only the outgoing lepton is detected the Green's function (GF) model [11, 12, 13, 14, 15, 16, 17] has been developed to describe FSI consistently with the exclusive scattering and using the same complex optical potential.

In the GF model, under suitable approximations, that are basically related to the IA, the components of the hadron tensor are written in terms of the s.p. optical model Green's function, whose self-energy is the Feshbach optical potential. The explicit calculation of the s.p. Green's function can be avoided by its spectral representation, that is based on a biorthogonal expansion in terms of a non Hermitian optical potential \mathcal{H} and of its Hermitian conjugate \mathcal{H}^\dagger . Calculations require matrix elements of the same type as the DWIA ones in Eq. 2, but involve eigenfunctions of both \mathcal{H} and \mathcal{H}^\dagger , where the imaginary part gives in one case an absorption and in the other case a gain of flux, and in the sum over n the total flux is redistributed and conserved. The GF approach guarantees a consistent treatment of FSI in the exclusive and in the inclusive scattering and gives a good description of (e, e') data [11, 12].

For the inclusive electron scattering both nonrelativistic GF [11, 15] and relativistic RGF [12]

approaches have been considered. For CC neutrino scattering the RGF model has been adopted. A numerical example is shown in Fig. 1 for the $^{12}\text{C}(\nu_\mu, \mu^-)$ cross sections calculated for an incident neutrino energy of $E_\nu = 1000$ MeV and two values of the muon scattering angle, *i.e.*, $\vartheta = 45^\circ$ (upper panel) and 135° (lower panel), as a function of the muon kinetic energy T_μ . In the case of the RGF model two different parameterizations of the relativistic optical potential have been used in the calculations, *i.e.*, the energy-dependent and A-dependent EDAD1 (RGF1) and the energy-dependent but A-independent EDAI (RGF-EDAI), which are fitted to proton elastic scattering data on several nuclei in an energy range up to 1040 MeV [18]. In Fig. 1 the RGF1 and RGF-EDAI results are compared with the results of the relativistic plane wave IA (RPWIA), where FSI are neglected, and with the cross sections obtained when only the real part of the relativistic optical potential (rROP) is retained and the imaginary part is neglected. The rROP approximation conserves the flux but, independently of its numerical results, it is conceptually wrong because the optical potential has to be complex owing to the presence of inelastic channels.

The differences between the rROP, RGF1, and RGF-EDAI results are essentially due to the imaginary part of the optical potential. Different parameterizations of the optical potential are available, that are able to give equivalently good descriptions of elastic proton-nucleus scattering data, but correspond to different optical potentials that mainly differ for their imaginary part. The imaginary part accounts for the overall effects of inelastic channels and is not univocally determined from the elastic phenomenology. The real terms are very similar and the cross sections calculated in rROP are practically insensitive to the choice of the optical potential. In contrast, the imaginary part is sensitive to the parameterization of the ROP and gives the differences shown in the figure. The RGF1 and RGF-EDAI results at $\vartheta = 45^\circ$ have somewhat different shapes for high values of T_μ , *i.e.*, low values of the energy transferred. At $\vartheta = 135^\circ$ the differences are reduced but the magnitude of the cross sections is significantly reduced.

5. Comparison of relativistic models

The analysis of data for neutrino experiments requires a precise knowledge of lepton-nucleus cross sections, where uncertainties on nuclear effects are reduced as much as possible. To this aim, it is important to check the consistency of different models and the validity of the adopted approximations. The results of the relativistic models developed by the Pavia and the Madrid-Sevilla groups for the inclusive scattering have been compared in [19] for the inclusive electron scattering and in [20] for the inclusive CC neutrino scattering. As a first step, the consistency of the RPWIA and rROP calculations performed by the two groups with independent numerical programs and with the same theoretical ingredients has been checked. Almost identical results are obtained in RPWIA and very similar results in rROP. This result gives us confidence on the reliability of our calculations and allows us to extend the comparison to the different descriptions of FSI.

An example is shown in Fig. 2, where the $^{12}\text{C}(e, e')$ cross sections obtained by the two groups in RPWIA and rROP are compared with the RGF results obtained with two different energy-dependent and A-dependent parameterizations for the relativistic optical potential of [18], *i.e.*, the EDAD1 (RGF1), already considered for the calculations shown in Fig. 1, and the EDAD2 (RGF2), and with the results of the relativistic mean field (RMF) model [21] of the Madrid-Sevilla group, where the scattering wave functions are calculated with the same strong real mean-field potential used for the initial bound states. The RMF model fulfills the dispersion relation and maintains the continuity equation.

The differences between the RMF and RGF results increase with the momentum transfer. Also the discrepancies between the RGF1 and RGF2 cross sections depend on the momentum transfer. At $q = 500$ MeV/ c the three results are similar, both in magnitude and shape, larger differences are obtained at $q = 1000$ MeV/ c . The shape of the RMF cross section shows an

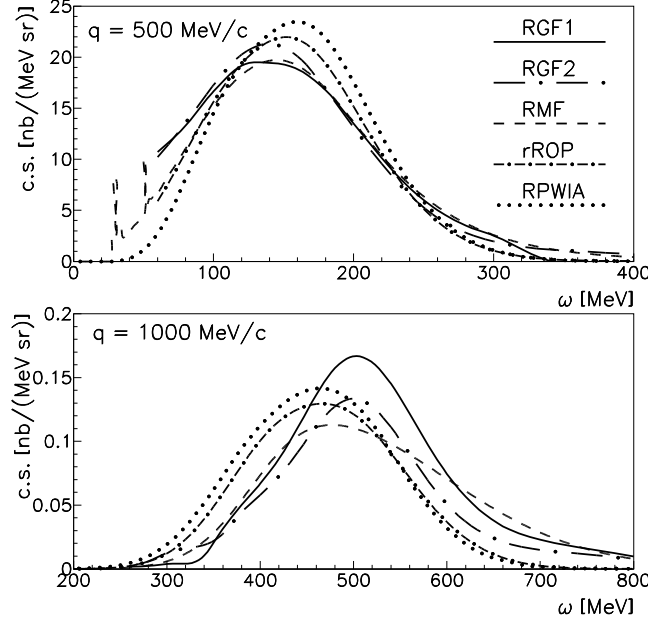


Figure 2. Differential cross section of the $^{12}\text{C}(e, e')$ reaction for an incident electron energy $\varepsilon = 1$ GeV and $q = 500$ and 1000 MeV/c. Results for RPWIA (dotted), rROP (dot-dashed), RGF1 (solid), RGF2 (long dot-dashed), and RMF (dashed) are compared.

asymmetry, with a long tail extending towards higher values of ω , that is essentially due to the strong energy-independent scalar and vector potentials present in the RMF model. The asymmetry towards higher ω is less significant but still visible for RGF1 and RGF2, whose cross sections show a similar shape but with a significant difference in the magnitude. At $q = 1000$ MeV/c both RGF1 and RGF2 cross sections are higher than the RMF one in the region where the maximum occurs. A stronger enhancement is obtained with RGF1, which at the peak overshoots the RMF cross section up to 40% and it is even higher than the RPWIA result.

The behavior of the RMF and RGF results as a function of q and ω is linked to the structure of the relativistic potentials involved in the RMF and RGF models. Whereas RMF is based on the use of a strong energy-independent real potential, RGF makes use of a complex energy-dependent optical potential. In RGF calculations the behavior of the optical potential changes with the momentum and energy transferred in the process, and higher values of q and ω correspond to higher energies for the optical potential. The RGF results are consistent with the general behavior of the optical potentials and are basically due to their imaginary part. The real terms of the relativistic optical potentials are very similar for the different parameterizations and the rROP cross sections do not show sensitivity to the particular parameterization considered. On the other hand, the energy-dependent scalar and vector components of the real part of the ROP get smaller with increasing energies. Thus the rROP result approaches the RPWIA one for large values of ω . In contrast, the imaginary (scalar and vector) part presents its maximum strength around 500 MeV, being also sensitive to the particular ROP parameterization. This explains the differences observed between the rROP and the two RGF results as a function of ω and q .

In Fig. 3 the RGF1, RGF2, and RMF results are compared with the experimental cross sections for three different kinematics [22, 23, 24]. The three models lead to similar cross sections. The main differences are obtained for higher values of the momentum transfer, about 800 MeV/c (bottom panel), where the RGF1 cross section (solid line) is larger than the RGF2

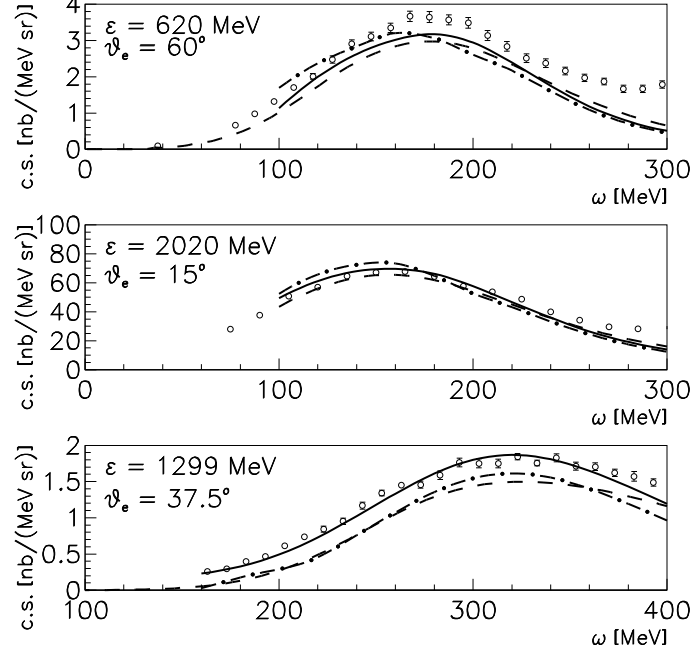


Figure 3. Differential cross section of the $^{12}\text{C}(e, e')$ reaction for different beam energies and electron-scattering angles in RGF1 (solid), RGF2 (long dot-dashed), RMF (dashed). Experimental data from [22, 23, 24].

(dot-dashed) and RMF (dashed) ones. The experimental cross section is slightly underpredicted in the top panel and well described in the middle panel by all calculations. Finally, results in the bottom panel show a fair agreement with data in the case of RGF1, whereas RGF2 and RMF underpredict the experiment. Although satisfactory on general grounds, the comparison with data gives only an indication and cannot be conclusive until contributions beyond the QE peak, like meson-exchange currents and Delta effects, which may play a significant role in the analysis of data even at the maximum of the QE peak, are carefully evaluated [25, 26, 27].

In Fig. 4 the $^{12}\text{C}(\nu_\mu, \mu^-)$ cross section obtained by the two groups in RPWIA and rROP in a kinematics with a fixed value of the incident neutrino energy, $E_\nu = 1000$ MeV, and two values of the momentum transfer, *i.e.*, $q = 500$ and 1000 MeV/ c , are compared with the corresponding RMF, RGF1 and RGF-EDAI results.

The cross sections shown in Fig. 4 are calculated with same incident lepton energy and momentum transfer as in the (e, e') calculations of Fig. 2. This is a kinematics more typical of electron-scattering experiments than of neutrino experiments, but the calculations have been carried out to perform a more direct comparison between the results of the models in electron and neutrino scattering. Actually, in the case of CC neutrino scattering the muon mass gives a different kinematics, with different values of the energy transfer and, as a consequence, of the energies of the outgoing nucleon. This means that in the RGF model the optical potential is calculated for electron and neutrino scattering at different energies. We have checked that if we reproduce the kinematics of electron scattering and perform calculations for the (ν_μ, μ^-) reaction with vanishing muon mass, the main difference with respect to the calculations shown in Fig. 4 is a shift of the cross section by about 100 MeV towards higher values of T_μ , without

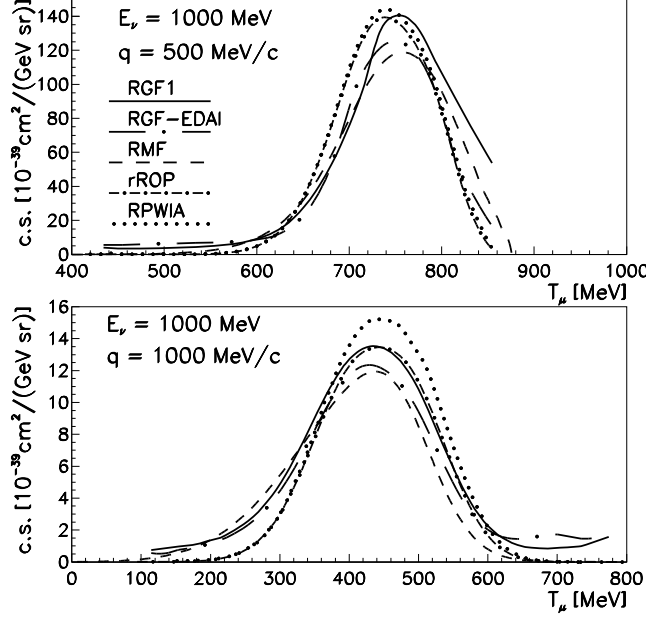


Figure 4. Differential cross section of the $^{12}\text{C}(\nu_\mu, \mu^-)$ reaction for $E_\nu = 1000$ MeV and $q = 500$ MeV/c and 1000 MeV/c. Results for RPWIA (dotted), rROP (dot-dashed), RGF1 (solid), RGF- EDAI (long dot-dashed), and RMF (dashed) are compared.

any significant change in the shape or in the strength.

Also for the results in Fig. 4 the shape of the RMF cross section shows an asymmetry with a tail extending towards higher values of ω (corresponding to lower values of the kinetic energy of the outgoing muon T_μ). An asymmetric shape towards higher ω is shown also by the RGF cross sections, while no visible asymmetry is given by the RPWIA and rROP results. Also in this case the significant differences obtained between the RGF and rROP cross sections are consistent with the general behavior of the phenomenological energy-dependent relativistic optical potentials and are basically due to their different imaginary part. As already shown for (e, e') reactions, the RGF yields in general a larger cross section than the RMF. The RGF and the RMF yield similar predictions, within a few percent for low- q , while as q goes up the RGF yields increasingly larger cross sections than RMF. This may reflect the influence of the pionic degrees of freedom, that can be included in a phenomenological way in the imaginary part of the optical potential [19, 20].

The results in Fig. 4 present some differences with respect to the corresponding cross sections of the inclusive electron scattering shown in Fig. 2. In both cases the differences between the results of the different models are generally larger for increasing value of the momentum transfer. For neutrino scattering, however, such a behavior is less evident and clear. In particular, the RGF1 cross section at $q = 1000$ MeV/c does not show the strong enhancement in the region of the maximum that is found for the (e, e') calculations of Fig. 2, where the RGF1 result is even larger than the RPWIA one. In the case of neutrino scattering the RGF results in the region of the maximum are generally larger than the RMF ones, but smaller than the RPWIA cross sections.

In spite of many similarities, inclusive electron scattering and CC neutrino-nucleus scattering are two different processes and caution should be drawn on their comparison. The different currents and their possible interplay with the other ingredients of the models do not allow an

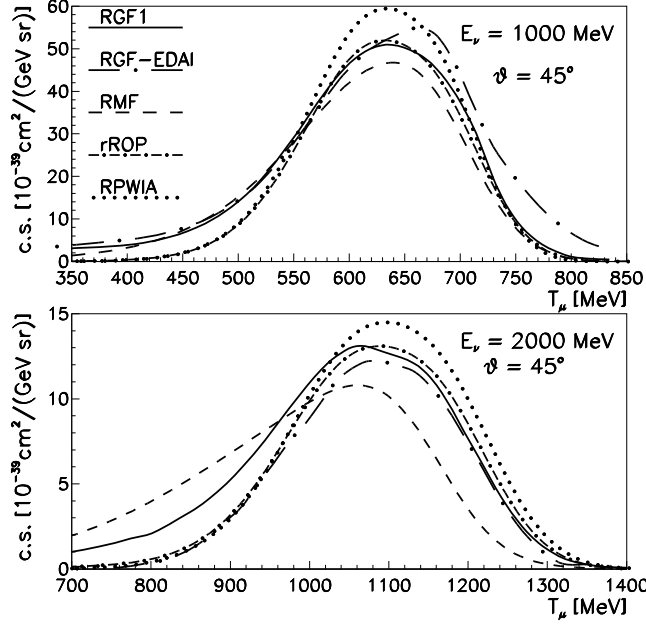


Figure 5. Differential cross section of the $^{12}\text{C}(\nu_\mu, \mu^-)$ reaction for $E_\nu = 1000$ MeV and 2000 MeV, and scattering angle $\vartheta = 45^\circ$. Results for RPWIA (dotted), rROP (dot-dashed), RGF1 (solid), RGF-EDAI (long dot-dashed), and RMF (dashed) are compared.

easy comparison. The numerical differences between the RGF results for electron and neutrino scattering can mainly be ascribed to the combined effects of the weak current, in particular its axial term, and the imaginary part of the ROP. We have checked that these effects can explain the fact that in neutrino scattering the RGF1 result does not give the strong enhancement in the region of the maximum that is obtained for the (e, e') cross section in Fig. 2.

The $^{12}\text{C}(\nu_\mu, \mu^-)$ cross section for the kinematics with $E_\nu = 1000$ and 2000 MeV and $\vartheta = 45^\circ$ are presented in Fig. 5. In these kinematics, that are more similar to those actually explored at present neutrino experiment facilities, the momentum transfer is not fixed and its value around the peak of the cross section is usually large, *i.e.*, $q \approx 700$ MeV/ c for $E_\nu = 1000$ MeV and $q \approx 1400$ MeV/ c for $E_\nu = 2000$ MeV. The shape of the RMF cross section shows also in this case an asymmetry, with a long tail extending towards lower values of T_μ , which is due to the strong energy-independent scalar and vector potentials present in the RMF approach. The asymmetry increases with larger incident neutrino energies. For the RGF cross sections the asymmetry is less significant but still visible, while almost no asymmetry is found for the RPWIA and rROP cross sections. The RGF1 and RGF-EDAI cross sections have somewhat different shapes, that are particularly visible for low ω at $E_\nu = 1000$ MeV and for higher ω at $E_\nu = 2000$ MeV. These differences are essentially due to the imaginary part of the ROP, that is sensitive to the particular parametrization considered, while the real terms of the ROP's are very similar for different parameterizations and give very similar results.

6. Comparison with Charged-Current Quasielastic MiniBooNE data

The double-differential cross sections for muon neutrino CC quasielastic (CCQE) scattering have recently been measured by the MiniBooNE collaboration [28]. These data have raised a strong debate over the role of the theoretical ingredients entering the description of the reaction. The

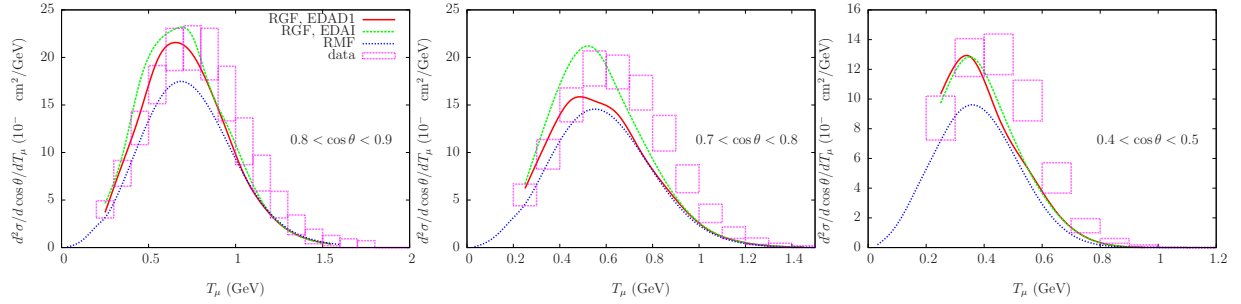


Figure 6. Flux-averaged double-differential cross section per target nucleon for the CCQE $^{12}\text{C}(\nu_\mu, \mu^-)$ reaction calculated in the RMF (blue line), the RGF1 (red), and RGF-EDAI (green) and displayed versus T_μ for various bins of $\cos \theta$. In all the calculations the standard value of the nucleon axial mass, *i.e.*, $M_A = 1.03 \text{ GeV}/c^2$ has been used. The data are from MiniBooNE [28].

experimental cross section is underestimated by the relativistic Fermi Gas (RFG) model, and also by the results of other more sophisticated models, unless the value of nucleon axial mass M_A is significantly enlarged ($1.35 \text{ GeV}/c^2$ in the RFG) with respect to the accepted world average value ($1.03 \text{ GeV}/c^2$ [29, 30]). Before drawing conclusions about the need to increase the axial mass it is however important to evaluate carefully the contributions of all nuclear effects.

Within the QE kinematic domain the treatment of FSI is essential for the comparison with data. The comparison between the results of the RMF and RGF models, where FSI are described by very different ingredients, can be helpful for a deeper understanding of the role played by FSI in the analysis of CCQE data and its influence in studies of neutrino oscillations at intermediate to high energies. The predictions of the two models have been compared with the recent CCQE MiniBooNE data [31].

The CCQE double-differential $^{12}\text{C}(\nu_\mu, \mu^-)$ cross sections averaged over the neutrino flux as a function of T_μ for various bins of $\cos \theta$, where θ is the muon scattering angle, are shown in Fig. 6. The RMF results yield reasonable agreement with data for small angles and low muon energies, the discrepancy becoming larger as θ and T_μ increase. The shape followed by the RMF cross sections fits well the slope shown by the data. A good agreement with the experimental shape is shown also by the RGF cross sections. The RMF and RGF models yield close predictions at larger values of T_μ , for all the bins of $\cos \theta$ shown in the figure. The RGF cross sections are generally larger than the RMF ones. The differences increase approaching the peak region, where the additional strength shown by the RGF produces cross sections in reasonable agreement with the data.

Also the differences between the RGF results with the two optical potentials are enhanced in the peak region, but remain in general within the uncertainties of the experimental errors. The EDAD1 and EDAI potentials yield close predictions for the bin $0.4 < \cos \theta < 0.5$, the differences are visible but anyhow small for the bin $0.8 < \cos \theta < 0.9$, being the RGF-EDAI cross section larger than the RGF1 one, while the difference is sizeable for the bin $0.7 < \cos \theta < 0.8$, with the RGF1 result closer to the RMF than to the RGF-EDAI one.

In Fig. 7 the flux-averaged double-differential cross sections are plotted versus $\cos \theta$ for two bins of T_μ , *i.e.*, $0.2 < T_\mu < 0.3 \text{ GeV}$ and $0.6 < T_\mu < 0.7 \text{ GeV}$. The shape of the experimental cross section is well described by the models. The RMF results generally underestimate the data, especially for the lower muon energy values, the agreement improves as T_μ increases. The additional strength produced by the complex optical potential in the RGF gives a reasonable agreement with the size of the experimental cross section. The agreement is better for smaller angles while the data are slightly underpredicted as θ increases. The discrepancy is larger with

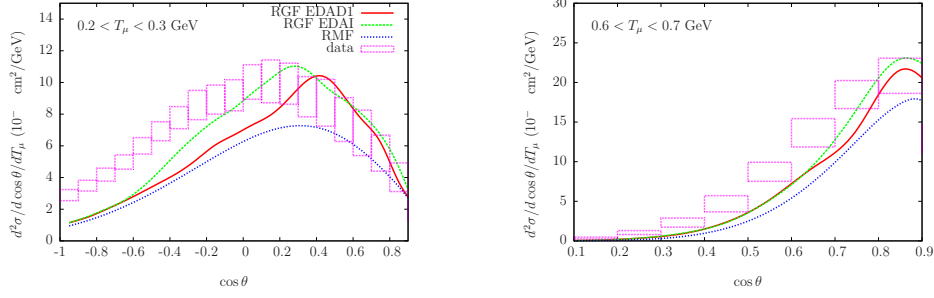


Figure 7. Flux-averaged double-differential cross section per target nucleon for the CCQE $^{12}\text{C}(\nu_\mu, \mu^-)$ reaction displayed versus $\cos\theta$ for two bins of T_μ . The results obtained with RMF (blue line), RGF1 (red), and RGF-EDAI (green) are compared. In all the calculations the standard value of the nucleon axial mass, *i.e.*, $M_A = 1.03 \text{ GeV}/c^2$ has been used. The data are from MiniBooNE [28].

RGF1, that gives in general a lower cross section than RGF-EDAI, and in the bin $0.2 < T_\mu < 0.3 \text{ GeV}$.

These results give further and clear indication that before drawing conclusions about the comparison with data and about the need to increase the value of the nucleon axial mass a careful evaluation of all nuclear effects is required. Important contributions can be produced by FSI. Both RGF and RMF models, where FSI are described with very different theoretical ingredients, give a good description of the shape of the experimental cross sections. The RMF generally underpredicts the data, but for lower values of the muon energy and scattering angle. In contrast, the RGF model can give cross sections of the same magnitude as the experimental ones without the need to increase the standard value of the axial mass. The larger cross sections in the RGF model are produced by the imaginary part of the ROP, that includes the overall effect of inelastic (nucleonic and non-nucleonic) channels and that is not univocally determined from the elastic phenomenology. The choice of the optical potential and a more refined determination of its imaginary part can deserve further investigation. Other contributions, not included in the present calculations, might play an important role in the analysis of CCQE data. Results of different models indicate that significant effects can be expected from correlations and meson-exchange currents [32, 33] or multiple knockout excitations [34, 35, 36, 37]. More refined calculations including all these contributions should be performed, but any new contribution should be included consistently in a model.

Acknowledgments

The authors wish to acknowledge the collaborations that have produced the results reported in this contribution. In particular, we are grateful to Franco Pacati, Franco Capuzzi, Juan Antonio Caballero, José Manuel Udías, and Maria Barbaro for fruitful collaborations.

References

- [1] Boffi S, Giusti C and Pacati F D 1993 *Phys. Rep.* **226** 1
- [2] Boffi S, Giusti C, Pacati F D and Radici M 1996 *Electromagnetic Response of Atomic Nuclei* Oxford Studies in Nuclear Physics, Vol. 20 (Oxford: Clarendon Press)
- [3] Boffi S, Cannata F, Capuzzi F, Giusti C and Pacati F D 1982 *Nucl. Phys. A* **379** 509
- [4] Meucci A, Giusti C and Pacati F D 2001 *Phys. Rev. C* **64** 014604
- [5] Udías J M, Sarriguren P, Moya de Guerra E, Garrido E and Caballero J A 1993 *Phys. Rev. C* **48** 2731
- [6] Radici M, Meucci A and Dickhoff W H 2003 *Eur. Phys. J. A* **17** 65
- [7] Giusti C, Meucci A, Pacati F D, Co' G and De Donno V 2011 *Preprint* arXiv:1105.1295 [nucl-th]
- [8] Meucci A, Giusti C and Pacati F D 2004 *Nucl. Phys. A* **744** 307

- [9] Meucci A, Giusti C and Pacati F D 2006 *Nucl. Phys. A* **773** 250
- [10] Meucci A, Giusti C and Pacati 2008 *Phys. Rev. C* **77** 034606
- [11] Capuzzi F, Giusti C and Pacati F D 1991 *Nucl. Phys. A* **524** 681
- [12] Meucci A, Capuzzi F, Giusti C and Pacati F D 2003 *Phys. Rev. C* **67** 054601
- [13] Meucci A, Giusti C and Pacati F D 2004 *Nucl. Phys. A* **739** 277
- [14] Meucci A, Giusti C and Pacati F D 2005 *Nucl. Phys. A* **756** 359
- [15] Capuzzi F, Giusti C, Pacati F D and Kadrev D N 2005 *Ann. Phys.* **317** 492
- [16] Meucci A, Giusti C and Pacati F D 2006 *Acta Phys. Polon. B* **37** 2279
- [17] Meucci A, Giusti C and Pacati F D 2009 *Acta Phys. Polon. B* **40** 2579
- [18] Cooper E D, Hama S, Clark B C and Mercer R L 1993 *Phys. Rev. C* **47** 297
- [19] Meucci A, Caballero J A, Giusti C, Pacati F D and Udías J M 2009 *Phys. Rev. C* **80** 024605
- [20] Meucci A, Caballero J A, Giusti C and Udías J M 2011 *Phys. Rev. C* **83** 064614
- [21] Caballero J A, Amaro J E, Barbaro M B, Donnelly T W, Maieron C and Udías J M 2005 *Phys. Rev. Lett.* **95** 252502
- [22] Barreau P *et al.* 1983 *Nucl. Phys. A* **402** 277
- [23] Day D B *et al.* 1993 *Phys. Rev. C* **48** 1849
- [24] Sealock R *et al.* 1989 *Phys. Rev. Lett.* **62** 1350
- [25] Barbaro M B, Caballero J A, Donnelly T W and Maieron C 2004 *Phys. Rev. C* **69** 035502
- [26] Amaro J E, Barbaro M B, Caballero J A, Donnelly T W, Molinari A and Sick I 2005 *Phys. Rev. C* **71** 015501
- [27] Ivanov M V *et al.* 2008 *Phys. Rev. C* **77** 034612
- [28] Aguilar-Arevalo A A *et al.* [MiniBooNE Collaboration] 2010 *Phys. Rev. D* **81** 092005
- [29] Bernard V, Elouadrhiri L and Meissner U G 2002 *J. Phys. G* **28** R1
- [30] Bodek A, Avvakumov S, Bradford R and Budd H 2008 *Eur. Phys. J. C* **53** 349
- [31] Meucci A, Barbaro M B, Caballero J A, Giusti C and Udías J M 2011 *Preprint* arXiv:1107.5145 [nucl-th]
- [32] Amaro J E, Barbaro M B, Caballero J A and Donnelly 2011 *Phys. Lett. B* **696** 151
- [33] Amaro J E, Barbaro M B, Caballero J A, Donnelly and Udías J M 2011 *Preprint* arXiv:1104.5446 [nucl-th]
- [34] Martini M, Ericson M, Chanfray G and Marteau J 2009 *Phys. Rev. C* **80** 065501
- [35] Martini M, Ericson M, Chanfray G and Marteau J 2010 *Phys. Rev. C* **81** 045502
- [36] Nieves J, Ruiz Simo I and Vicente Vacas M J 2011 *Phys. Rev. C* **83** 045501
- [37] Nieves J, Ruiz Simo I and Vicente Vacas M J 2011 *Preprint* arXiv:1106.5374 [nucl-th]